Proceedings of the ASME 2011 Turbine Technical Conference and Exposition
ASME Turbo Expo 2011
June 6-10, 2011, Vancouver, Canada

DRAFT: GT2011-45852

DRAFT: ACTUATED TRANSITION IN AN LP TURBINE LAMINAR SEPARATION: AN EXPERIMENTAL APPROACH

Jenny Baumann*
Martin Rose, Tobias Ries, Stephan Staudacher
Institute of Aircraft Propulsion Systems
Universität Stuttgart
Stuttgart, 70569
Germany
Email: baumann@ila.uni-stuttgart.de

Ulrich Rist
Institute of Aerodynamics and Gas Dynamics
Universität Stuttgart
Stuttgart, 70569
Germany

ABSTRACT

The reduction of blade counts in the LP turbine is one possibility to cut down weight and therewith costs. At low Reynolds numbers the suction side laminar boundary layer of high lift LP turbine blades tends to separate and hence cause losses in turbine performance. To limit these losses, the control of laminar separation bubbles has been the subject of many studies in recent years.

A project is underway at the University of Stuttgart that aims to suppress laminar separation at low Reynolds numbers (60,000) by means of actuated transition. In an experiment a separating flow is influenced by disturbances, small in amplitude and of a certain frequency, which are introduced upstream of the separation point. Small existing disturbances are therewith amplified, leading to earlier transition and a more stable boundary layer. The separation bubble thus gets smaller without need of a high air mass flow as for steady blowing or pulsed vortex generating jets.

Frequency and amplitude are the parameters of actuation. The non-dimensional actuation frequency is varied from 0.2 *to* 0.5*, whereas the normalized amplitude is altered between* 5*,* 10 *and* 25 *% of the free stream velocity. Experimental investigations are made by means of PIV and hot wire measurements. Disturbed flow fields will be compared to an undisturbed one. The effectiveness of the presented boundary layer control will be compared to those of conventional ones. Phase-logged data will give an impression of the physical processes in the actuated flow.*

NOMENCLATURE

a_{act}	actuation amplitude [m/s]
$\tilde{a}_{\text{act}}$	non-dimensional amplitude a_{act}/U_∞ [-]
H_{12}	shape parameter [-]
f_{act}	actuation frequency [Hz]
p	(static) pressure [Pa]
Re	Reynolds number [-]
l_{s}	chord length [mm]
Sr_{act}	Strouhal number of actuation [-]
T	temperature [K]
Tu	turbulence level [%]
U_∞	free stream velocity [m/s]
u,v,w	velocity components in x-, y- and z-direction [m/s]
x,y,z	streamwise, wall-normal and spanwise coordinate [mm]
$\tilde{x},\tilde{y}$	non-dimensional coordinates $x/l_s, y/l_s$ [-]

Greek Symbols

δ_1	displacement thickness [mm]
δ_2	momentum thickness [mm]
η	dynamic viscosity [kg/ms]
ρ	density [kg/m^3]
ϕ	phase angle of sine wave [°]
ψ	stream function [m^2/s]

*Address all correspondence to this author.

Indices

act	actuation
Bl1,2	boundary layer bleeds
in	inlet
P	inlet plenum
TE	trailing edge
TS	test section

INTRODUCTION

The trend in modern engine design, in addition to increases in the overall engine efficiency, is to reduce the weight and complexity of its components (see Ardey et al. [1]). Therefore stage numbers and blade numbers of Low Pressure Turbines (LPT) are reduced, leading to a reduction of row solidity. At the same time the bypass ratio is increased. Hence LP turbines are to drive larger fans at lower fan speeds. Due to low Reynolds numbers (*Re*) of about $60,000$ in small, high flying business jets or micro gas turbines as used in Unmanned Aerial Vehicles, the laminar boundary layer in those LP turbines is more likely to separate than for larger *Re*. Laminar separation causes reduction in turbine performance and with it overall engine performance. Therefore laminar separation bubbles (LSB) should be avoided. Many investigations on separation control have been published. These investigations can be described as either passive or active flow control. Passive flow control devices, such as turbulence trips or vortex generators, were recently investigated by Himmel et al. [2] and McAuliffe and Yaras [3]. Those devices cannot adapt themselves to changing operation conditions which may negatively affect the performance under off-design conditions. Active separation control such as vortex generating jets (VGJ) was investigated amongst others by Schumann [4], Volino [5], Rivir et al. [6], Gross and Fasel [7] and Bons et al. [8]. The synthetic jets are used to form streamwise vortices which transport fluid of high kinetic energy into the separation bubble to minimize or even eliminate it. As demonstrated by Rivir et al. [6] the loss coefficient can be reduced up to $40-50\,\%$ at a blowing ratio of 2. Yet the high energetic flow has to be bleeded off the compressor and thus is taken from the energy winning process. The idea of pulsed VGJs therefore has been raised. Given that the mass flow is considerably reduced, pulsed jets have been found to be more effective than steady blowing jets. This was demonstrated by Bons et al. [9] and Volino et al. [10].

Stieger and Hodson [11] found out that periodically appearing and disappearing separation bubbles exert less dissipation loss than fully turbulent boundary layers. This leads to the hypothesis that active separation control in LP turbines is capable of reducing dissipation losses.

In the present study small disturbances with ideally zero net mass flow of distinct frequencies and small amplitudes are considered. These disturbances accelerate the laminar to turbulent transition process whereby earlier transition leads to a reduced separation. This effect has been investigated by Rist and Augustin [12] and Ricci et al. [13]. The latter study was about the boundary layer on wings. For this work the combination of PIV and hot wire measurements in a low-speed wind tunnel will give a fundamental understanding of the processes leading to a suppression of the separation bubble in a disturbed low pressure turbine. The pressure gradient of the LPT blade row is simulated in a wind tunnel by a profile on the opposite wall of a flat plate. A similar experimental setup has been successfully used before by Lang et al. [14] who investigated a LSB in a water channel.

In this study the profile produces a pressure distribution similar to the distribution in an LPT. A separation bubble forms on the flat plate which is to be influenced by disturbances, small in amplitude and of a certain frequency, brought in shortly before the separation bubble. The disturbances, promoting the Kelvin-Helmholtz instability of the shear layer of the separation, are amplified. Through this amplification process the boundary layer gets more stable and the separation bubble gets smaller without need of a large air mass flow as for vortex generating jet control. Numerical investigations by means of URANS and DNS that were done prior to the presented work as well as preliminary experimental results were published by Ries et al. and Baumann et al. in [15–17]. Experimental results showing the effect of actuation on the boundary layer are presented here.

EXPERIMENTAL SETUP

The experimental setup consists of three main components: the wind tunnel system, the actuation system and the measurement systems.

Wind Tunnel System

The experimental investigations are done in a wind tunnel working in suction mode that is driven by a vacuum pump. It can be split up into the subsystems of inlet plenum, test section and pipework. A schematic of the wind tunnel system can be seen in Fig. 1.

Inlet Plenum Air is sucked from the large test hall, where other test stands are located, forklifts run and people work. Therefore it is inevitable to have a settling chamber (inlet plenum) upstream of the test section which eliminates the disturbances in the test hall air. The ratio of inlet plenum to test section cross section is $A_\mathrm{P}/A_\mathrm{TS} = 20/1$. In contrast to usual laminar flow test rigs the inlet of this plenum is very small, even smaller than the cross section of the tunnel. The velocity of the sucked air is highly increased by forcing it through a small hole with $A_\mathrm{in}/A_\mathrm{TS} = 1/10$. Influences of environmental disturbances on the flow in the test rig are therewith eliminated. Perforated baffle plates force the fluid to spread over the entire cross section

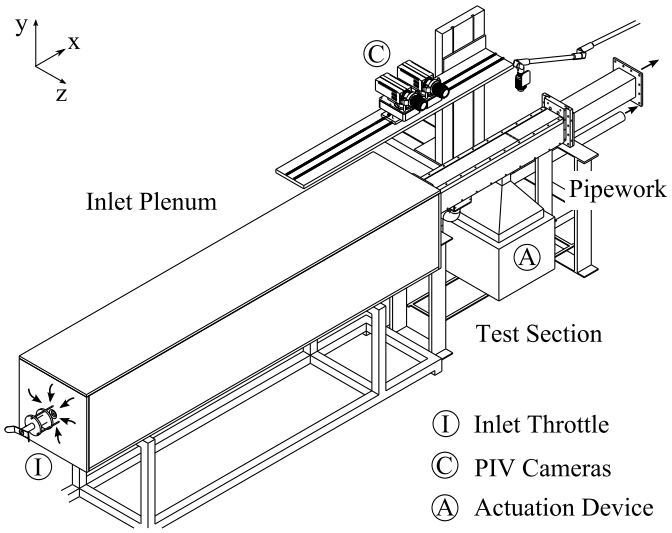

FIGURE 1. EXPERIMENTAL SETUP

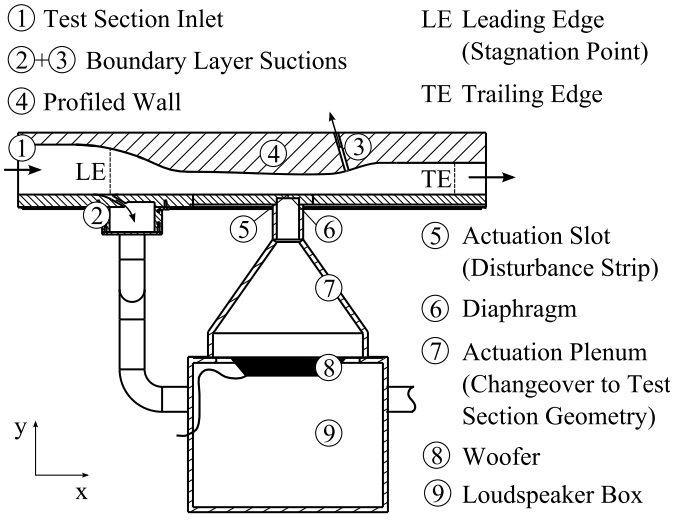

FIGURE 2. TEST SECTION AND ACTUATION DEVICE

of the plenum and thereby reduce the speed of the flow. The low speed flow is made uniform by the aid of honeycombs and fabric screens. As a result, strong turbulence produced by the unusual inlet design is damped out and the turbulence level in the inlet of the test section reaches $Tu = 0.5\,\%$. A sine-cosine passage at the rear of the plenum reduces the cross section to those of the test section. It was designed considering curvature to enable accelerated flow that is unlikely to separate.

The pressure drop across the inlet plenum is adjusted by a cone shaped device that can be moved in and out of the inlet hole as described by Baumann et al. [17]. Increasing the inlet velocity by decreasing the inlet area leads to higher losses in total pressure. The overall inlet plenum pressure drop can thus be varied from about 150 to 2000 Pa to countervail changing environmental conditions and preserve Reynolds number.

Test Section The experiment simulates the flow on an LP turbine blade suction side at low Reynolds numbers. The Reynolds number definition applied here is

$$Re = \frac{U_{\mathrm{TE}} \cdot l_{\mathrm{s}} \cdot \rho}{\eta}. \tag{1}$$

It is calculated by the chord length l_{s}, the main flow velocity U_{TE} at the trailing edge, the fluid density ρ and the dynamic viscosity η. The low Mach number and Reynolds number flow is modeled with a flat plate and an opposite contour which was designed with the aid of CFD calculations. The profile induces a pressure coefficient distribution on the opposite flat plate similar to those of a T161 blade profile suction side. The design procedure is described by Ries et al. [15].

The cross section area at the inlet of the test section is $100 \times 100\,\mathrm{mm}$ (see (1) in Fig. 2). While the width stays constant the height of the cross section is reduced to 31.9 % and then expanded again to 65 % of the inlet value. The total length of the test section is 1000 mm whereas the defined chord length is $l_{\mathrm{s}} = 677.93\,\mathrm{mm}$. The chord length starts at the leading edge (LE), at 19 % of total length, and ends at the defined location of trailing edge (TE), shortly upstream of the flange to the pipeline. Leading and trailing edge are shown in Fig. 2.

To ensure similarity to the turbine blade flow, boundary layer bleeds are located at two positions in the test section. The first one, on the bottom wall (2), enables a new starting boundary layer with defined stagnation point (leading edge). The second bleed on the top wall in the decelerated zone (3) pulls the flow towards the profile and forces the separation bubble to form on the flat plate. Locations of these two bleeds are at $x_{\mathrm{Bl1}}/l_{\mathrm{s}} = \tilde{x}_{\mathrm{Bl1}} = 0$ and $x_{\mathrm{Bl2}}/l_{\mathrm{s}} = \tilde{x}_{\mathrm{Bl2}} = 0.69$.

Pipes The parameter used to control the experiments is the Reynolds number according to Eqn. (1). Given that this study is about small Reynolds number flow and the test rig is large scale, velocities and therewith mass flow rates in the wind tunnel are very low ($U_\infty \leq 4\,\mathrm{m/s}$). However, the pressure ratio from atmosphere to vacuum pump inlet is very large ($p_\infty / p_{\mathrm{vacuum\ pump}} \approx 30$). Any mass flow control device must be choked, which is why mass flows are set up by orifice plates rather than valves. These orifices are located in the pipes downstream of the test section and were designed according to DIN EN ISO 5167-2. With orifice plates of different size, various operating points by means of Reynolds number and mass flow ratios can be set (see [17]).

Actuation System

To excite the laminar-turbulent transition process, disturbances of defined frequencies are to be introduced in the boundary layer. This actuation is realized by a loudspeaker device. It consists of a loudspeaker, a frequency generator, an amplifier and an oscilloscope.

A digital frequency generator (DFG) can be used to produce signals with wave forms of different shapes. The wave form for the experiment is a pure sine wave as the influence of only one frequency shall be investigated. Frequency and amplitude of the output signal can be set easily. Due to the fact that the amplitude of the signal is not sufficiently high for actuation, an amplifier is required. The amplification is adjusted stepwise which simplifies the reproduction of an actuation setup. As the amplifier has no display to show the output voltage, an oscilloscope is used to monitor the output signal.

A stability analysis in the location of the actuation slot results in possible frequencies for exciting transition. The analysis was done by Ries et al. [15, 16]. Given that these frequencies range from 25 to 85 Hz, depending on the Reynolds number in the flow, a woofer (300 W, 270 mm in diameter) was chosen to produce the signal. As is denoted in Fig. 2 the frequency generator is used to drive the woofer (8) sitting in a wooden loudspeaker box (9) underneath the test section. The air on top of the woofers membrane is forced to oscillate with the frequency of the loudspeaker. The sinusoidal signal then reaches a polyethylene diaphragm (6) which is attached to the slotted bottom plate of the test section. As polyethylene is very thin and also flexible, the diaphragm passes the signal through the actuation slot (5) into the test section. The area of the disturbance strip is 0.3×100 mm. The sensitivity of actuation location on actuation effectiveness was investigated by means of DNS calculations [16]. Starting at a location $\tilde{x}_{\text{act}} = 0.614$ for $Re = 79,000$, the impact of actuation location on the bubble was shown to be very small. Only moving the disturbance strip further downstream led to considerably less effective actuation. Therefore the location in experiment was fixed at $\tilde{x}_{\text{act}} = 0.516$ which is as near to $\tilde{x}_{\text{act}} = 0.614$ as it could be by reasons of wind tunnel design.

Measurement Systems

To monitor the operation point and calculate flow parameters of interest, a variety of measurement techniques are used.

Pressure and Temperature Measurement The Reynolds number is the parameter for real turbine flow analogy. By measuring pressure, temperature and humidity in the test rig mass flow rates and therewith Reynolds number can be calculated. Static pressure tappings are located in the inlet plenum and test section. For total pressure measurements Pitot probes are located upstream of each the orifice plates. The pressures are connected to a number of differential pressure transducers and

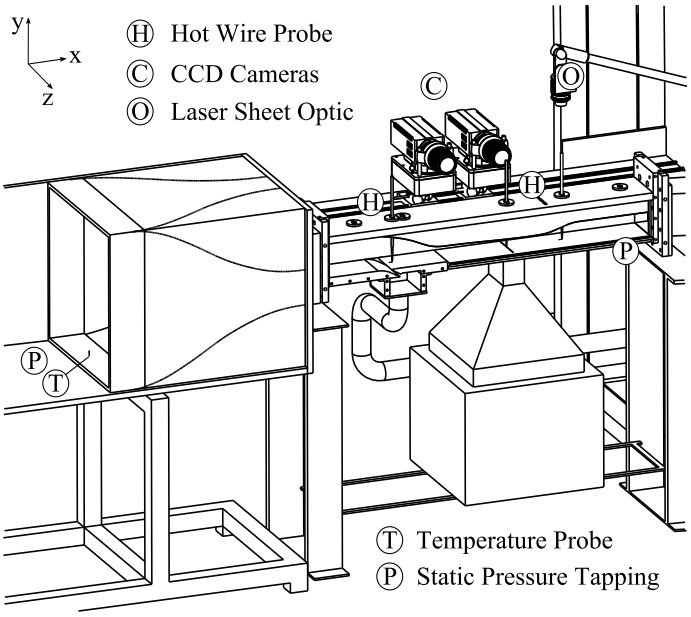

FIGURE 3. MEASUREMENT SYSTEMS AND LOCATIONS

measured against ambient pressure. The probes for ambient temperature and the temperature in the inlet plenum are thermocouples of type K. Locations of the temperature probe and the static pressure tappings in the test section respectively in the plenum are denoted in Fig. 3. It is assumed that the measured total temperature stays constant over the test section.

The uncertainty for pressure measurements is $\Delta p = \pm 1.5\,\%$. For temperature measurements it is $\Delta T = \pm 1.0\,\%$. The resulting Reynolds number uncertainty from measurements is 1.5 %. The variation of Re based on measurement uncertainties is smaller than its variation due to ambient conditions. Changes in ambient pressure that cannot be compensated by the inlet throttle cause Re variations of 3.5 %. This leads to a maximum total Reynolds number deviation of $\Delta Re = \pm 5\,\%$.

Constant Temperature Anemometry Hot wire probes are used to gain information about the turbulence in the flow field. Probe access holes are therefore located at certain positions on the profiled wall. The measurement system and the probes are from *DantecDynamics*, as well as the data acquisition software *StreamWare*. The measurements were taken at a frequency of 1 kHz with low pass filtering at 300 Hz.

The turbulence level Tu generally is calculated according to Eqn. (2) from the standard deviations of the measured velocity components u, v and w and the free stream velocity U_∞.

$$Tu = \frac{1}{U_\infty} \cdot \sqrt{\frac{1}{3} \cdot \left(\overline{u'^2} + \overline{v'^2} + \overline{w'^2} \right)} \tag{2}$$

The probes used are single-wired and hence only measure one velocity vertical to the wire. With this velocity, the turbulence level can be calculated according to Eqn. (3).

$$Tu = \frac{1}{U_\infty} \cdot \sqrt{\overline{u'^2}} \tag{3}$$

Like the measured velocity, Tu only represents fluctuations vertical to the wire. The z-wise component is neglected, which is sufficient for the 2D examination of the flow field.

Furthermore, hot wire measurements are taken for evaluation of the output signal from the actuation device. With an FFT analysis, the effective actuation amplitude can be gained. Additionally the quality of the signal by means of the height of its harmonics can be evaluated.

Particle Image Velocimetry To get a 2D flow field and a visual impression of the separation, Particle Image Velocimetry (PIV) is employed. In contrast to the depiction in Fig. 3, either hot wire or PIV measurements are taken. Thus there are two profiled walls, an aluminium one with the locations for hot wire probe access and an acrylic glass one for PIV measurements.

Data are taken with a measurement system from *LaVision*. For most of the investigations two CCD cameras with a resolution of 1600×1200 px each are used to permit a wider observation area (window size per camera 140×105 mm) and 2D velocities. The acquisition and processing of the data is done with the *DaVis* software. A set of 170 double frame pictures are taken at a frequency of about 8 Hz. Depending on the intent of the measurement, the acquisition frequency has to be chosen with reference to the actuation frequency.

Prior to processing a mask is created cutting off major reflexions in order to avoid errors from reflexions off the walls. The processing of the masked pictures is done using the cross-correlation mode and multiple pass iteration with decreasing interrogation window size from 64×64 px to 32×32 px. The window overlap is set to 50 %.

EXPERIMENTAL INVESTIGATIONS

Turbulence Level

The velocity profile and with it the turbulence level were evaluated from hot wire probe traverses in the spanwise center of the channel. These measurements were taken in different streamwise positions. Probe access locations can be seen in Fig. 3. A *DantecDynamics* 90° single wire probe type *55P14* was used for those measurements.

It was found that the free stream turbulence of $Tu \leq 0.5\,\%$ in the test section (measured at $\tilde{x} = -0.13$) is sufficiently small for laminar boundary conditions. The free stream turbulence at the location of separation (measured at $\tilde{x} = 0.752$) was found to be $Tu \approx 1\,\%$, which again is sufficiently small as the experiments are to be compared to turbomachinery flow.

Actuation Amplitude

To calibrate the actuation amplitude, hot wire measurements were taken at the location of the actuation in the absence of main stream flow. A straight single wired *DantecDynamics* probe type 55P11 was employed for that purpose. The hot wire was positioned in the streamwise and spanwise center of the actuation slot. As the amplitude decreases with increasing wall-normal distance to the slot, the measured signal is very sensitive to the y position of the wire. The distance should preferably be smaller than the slot width of 0.3 mm. Given that the positioning was done manually the location was chosen to be at a distance of approximately $0.3 - 0.5$ mm.

From measurements with different actuation frequencies, the three actuation amplitudes investigated are found to cover a range from $\tilde{a}_{\mathrm{act},1} \approx 5\,\%$ to $\tilde{a}_{\mathrm{act},3} \approx 25\,\%$ of the free stream velocity U_∞ at the streamwise location of the actuation slot. As U_∞ depends on the mass flow through the orifice plates, the non-dimensional actuation amplitude varies with changing orifice configuration. The normalized values including their variation thus are $\tilde{a}_{\mathrm{act},1} = 5 \pm 1\,\%$, $\tilde{a}_{\mathrm{act},2} = 10 \pm 2\,\%$ and $\tilde{a}_{\mathrm{act},3} = 25 \pm 5\,\%$. Due to a dependency of amplitude on the frequency of the DFG output signal, a variation of amplitude related to actuation frequency could be found. Compared to the variations with orifice configuration those from the frequency generator are negligible.

Time-Averaged PIV Results

Initial PIV measurements were used to find basic flow field orifice configurations. For a nominal Reynolds number of 60,000 three different configurations of mass flow ratio were chosen to be investigated. The related mass flow rates for each case are the following.

A) $\dot{m}_{\mathrm{Bl1}}/\dot{m}_{\mathrm{TE}} = 9.375\,\%$, $\dot{m}_{\mathrm{Bl2}}/\dot{m}_{\mathrm{TE}} = 2.7\,\%$
B) $\dot{m}_{\mathrm{Bl1}}/\dot{m}_{\mathrm{TE}} = 9.375\,\%$, $\dot{m}_{\mathrm{Bl2}}/\dot{m}_{\mathrm{TE}} = 2.0\,\%$
C) $\dot{m}_{\mathrm{Bl1}}/\dot{m}_{\mathrm{TE}} = 9.375\,\%$, $\dot{m}_{\mathrm{Bl2}}/\dot{m}_{\mathrm{TE}} = 1.5\,\%$

The first mass flow configuration produces a big separation bubble (case A). The second bubble is of moderate size (case B), whereas the third one is small (case C). For later comparison with measurements at different Reynolds numbers the Strouhal number Sr is used as a non-dimensional actuation frequency. It is calculated according to Eqn. (4) with actuation frequency f_{act}, chord length l_{s} and main flow velocity U_{TE} at the trailing edge.

$$Sr_{\mathrm{act}} = \frac{f_{\mathrm{act}} \cdot l_{\mathrm{s}}}{U_{\mathrm{TE}}} \tag{4}$$

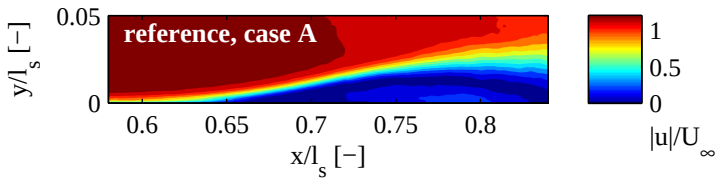

(a) consistent scale for x and y axis

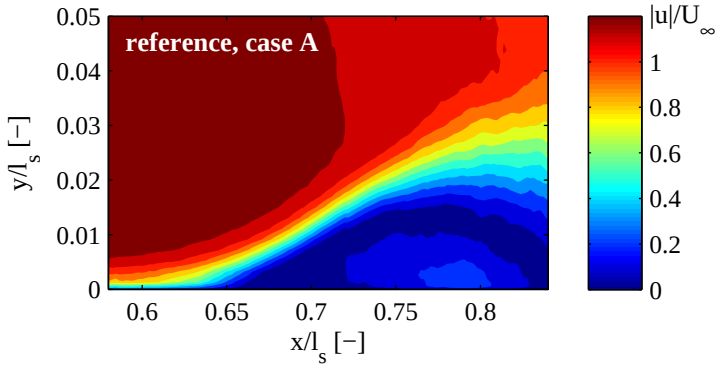

(b) dissimilar scale for x and y axis, y exaggerated

FIGURE 4. PIV TIME-AVERAGE VELOCITY MAGNITUDE, REFERENCE FIELD FOR CASE A WITH DIFFERENT SCALES

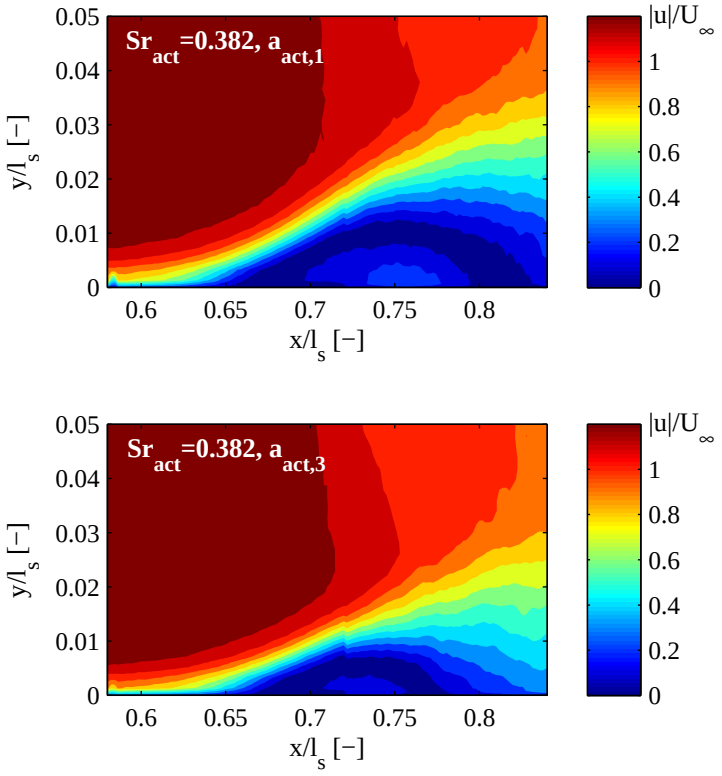

FIGURE 5. PIV TIME-AVERAGE VELOCITY MAGNITUDE, ACTUATED FIELDS FOR CASE A WITH $Sr_{\text{act}} = 0.382$ *(dissimilar scale)*

With the aid of stability analysis, the actuation Strouhal number range was found to be $0.2 \leq Sr_{\text{act}} \leq 0.5$ for the given Reynolds number of 60,000. All configurations were tested with and without actuation.

In the first measurement campaign time-averaged data were acquired. For that purpose the recording frequency for the PIV pictures was changed for each actuation frequency as it must not be a multiple of the actuation frequency f_{act}. That way an average separation bubble size for each case and actuation parameter configuration could be attained. In Fig. 4 the distribution of velocity vector magnitudes in a reference flow field of case A are displayed. Using consistent scales for the x and y axis leads to flat diagrams as can be seen in the upper subfigure (Fig. 4.a). As the intent of this paper is to show the influence of actuation on separation, the y scale is distended so that the separation bubble is exaggerated. All following figures displaying y/l_s over x/l_s will have similar scales.

The velocity vector magnitudes displayed in Fig. 4 were normalized with the free stream velocity U_∞, which was not necessarily the maximum velocity of the cross section. The observation area starts shortly downstream of the actuation slot ($\tilde{x}_{\text{act}} = 0.516$) and is focused on the separated zone. Data from two cameras were assembled. This explains the discontinuity at some points at $\tilde{x} \approx 0.72$.

This flow field was disturbed with different actuation configurations. In Fig. 5 the actuated flow fields of $Sr_{\text{act}} = 0.382$ with actuation amplitudes of $\tilde{a}_{\text{act},1}$ and $\tilde{a}_{\text{act},3}$ respectively are displayed. Both actuations visibly lead to a smaller separation. The reattachment happens earlier than in the reference case where the smallest velocity contour (dark blue) reattaches to the wall not until the end of the observation area. This effect is larger for the higher amplitude actuation shown in the bottom picture of Fig. 5.

Displacement Thickness and Shape Factor The results gained from PIV measurements are velocity vectors in a 2D flow field. As per Eqn. (5) and (6) the displacement thickness δ_1 and momentum thickness δ_2 can be calculated from the velocity data.

$$\delta_1 = \int_0^\infty \left(1 - \frac{u}{U_\infty}\right) dy \tag{5}$$

$$\delta_2 = \int_0^\infty \frac{u}{U_\infty} \cdot \left(1 - \frac{u}{U_\infty}\right) dy \tag{6}$$

The mainstream velocity U_∞ is a fixed value taken from the averaged PIV data and can vary between different measurement days or bubble sizes (case A-C).

Given that the processing of the PIV data only computes velocities at discrete points in the observation area, the integrals are not solved analytically but approximated by the trapezoidal rule. The ratio of δ_1 to δ_2 is defined as the shape factor H_{12}

$$H_{12} = \frac{\delta_1}{\delta_2}, \tag{7}$$

which is used to evaluate the nature of the boundary layer. In absence of a pressure gradient on a flat plate H_{12} is about 1.3 for a turbulent boundary layer, 2.54 for laminar a boundary layer and approximately 3.5 to 4.0 where the laminar boundary layer separates [18]. These numbers vary for a flat plate in presence of a pressure gradient but their magnitude still can be used as an indication for the different boundary layer types.

An example of actuated δ_1, δ_2 and H_{12} distributions in comparison to the reference case (bubble size A) is displayed in Fig. 6. The displacement thickness in the top diagram of Fig. 6 is relatively high with $\delta_{1,max} \approx 17\,\text{mm}$ for the reference case (black squares). With actuation the maximum value is reduced. An increase of actuation amplitude thereby leads to a higher displacement thickness reduction. The influence is biggest for the highest actuation amplitude $\tilde{a}_{\text{act},3}$ (red diamonds) where δ_1 is reduced to 9 mm. The maximum value of shape factor in the bottom diagram likewise is smallest for $\tilde{a}_{\text{act},3}$. In addition to the reduction of the maximum values of δ_1 and H_{12}, also the reattachment that is denoted by a reduction of H_{12} to a value of about 1.3 is reached at an earlier streamwise location.

Stream Function As can be seen in the diagram of shape factor distribution the momentum thickness definition is insignificant for a separated boundary layer where δ_2 decreases due to the reverse flow. Therefore H_{12} extravagates the defined values in the middle of the separated zone. Although the definition is valid again for the reattaching boundary layer, an additional parameter for separation bubble evaluation is introduced. The stream function ψ is calculated as per Eqn. (8).

$$\psi = \int u dy \tag{8}$$

For the same reasons as for δ_1 and δ_2, ψ is calculated by a summation rather than by numerical integration. According to Eqn. (9) a stream function value ψ_n can be calculated for each y-position.

$$\psi_n = \sum_{i=1}^{n} u_i \cdot \Delta y_i \tag{9}$$

Plotting the isolines of the calculated stream function field the separation bubble can be pictured. The separation (S) and

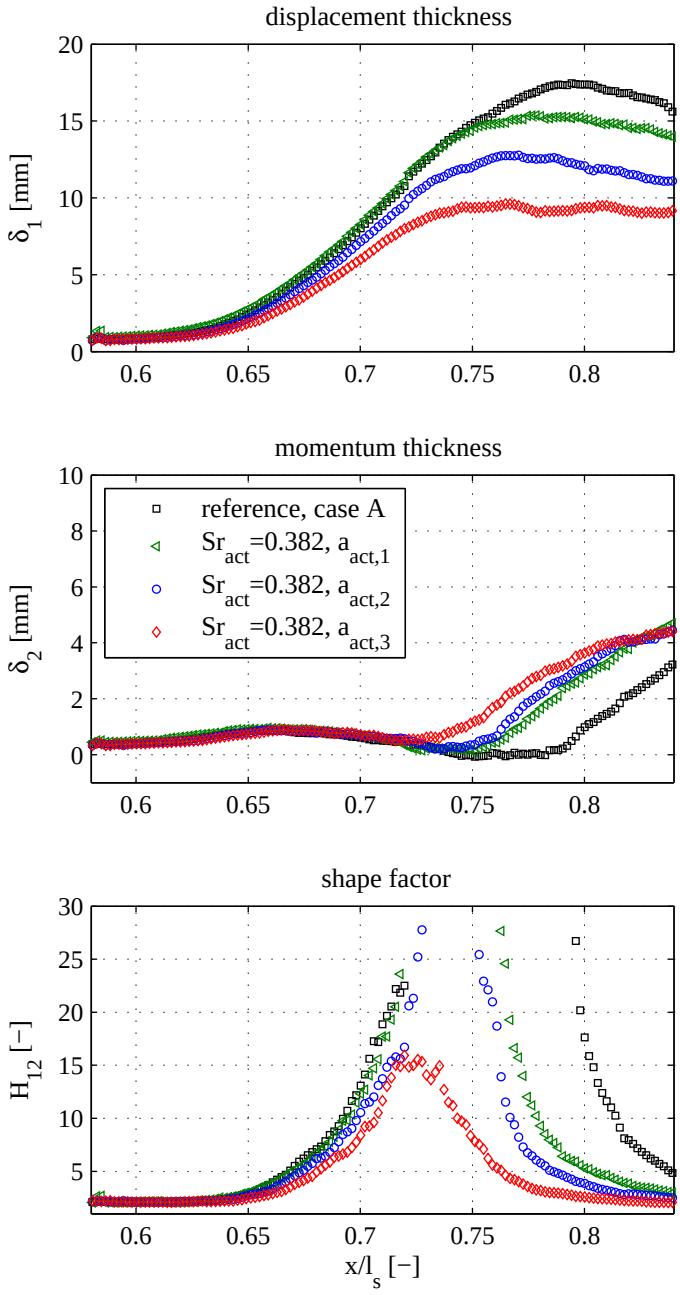

FIGURE 6. COMPARISON OF BOUNDARY LAYER PARAMETERS FOR CASE A WITH $Sr_{\text{act}} = 0.382$

reattachment point (R) are located where the separation streamline ($\psi = 0$) touches the wall. In Fig. 7 the separation streamlines for the reference and actuation cases are shown. The separation bubble for the reference case is biggest and does not reattach to the wall. With increasing actuation amplitude the separation point moves downstream and the enclosed area gets smaller.

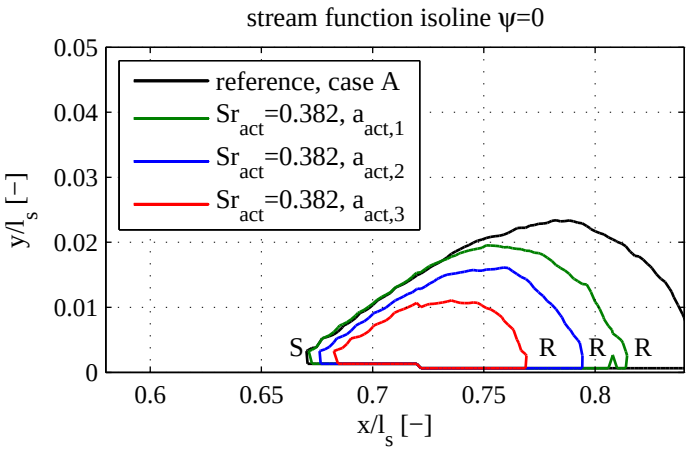

FIGURE 7. SEPARATION STREAMLINES FOR CASE A, $Sr_{\text{act}} = 0.382$ (S: SEPARATION, R: REATTACHMENT) *(dissimilar scale)*

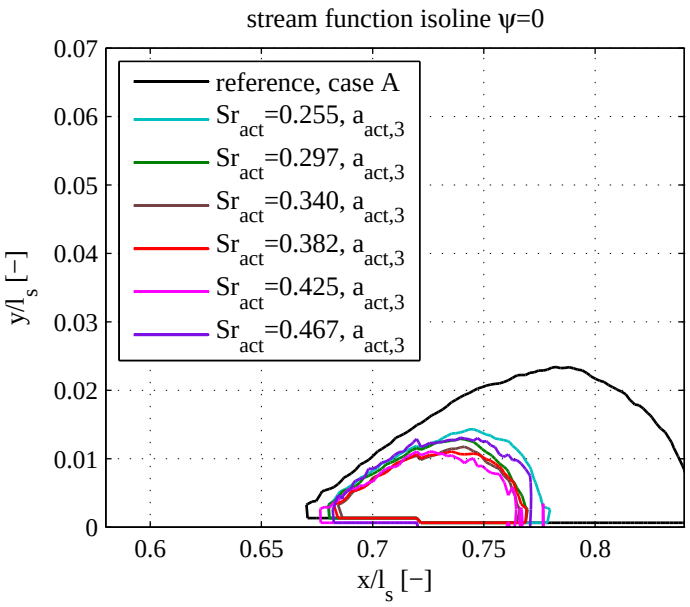

FIGURE 8. SEPARATION STREAMLINES FOR CASE A, $\tilde{a}_{\text{act},3}$ *(dissimilar scale)*

This leads to a major reduction of separation bubble size for the highest amplitude $\tilde{a}_{\text{act},3}$ (red line). The height of the separation thereby is reduced from 0.024 to 0.011 while the length is shortened from > 0.18 to 0.08.

Separation streamlines for different actuation Strouhal numbers and the amplitude $\tilde{a}_{\text{act},3}$ are displayed in Fig. 8. In comparison to Fig. 7 it can be seen that the effect of frequency variation is not as large as it is for amplitude. Yet, there is an optimal range at about $0.340 - 0.425$.

Additional measurements and corresponding calculations

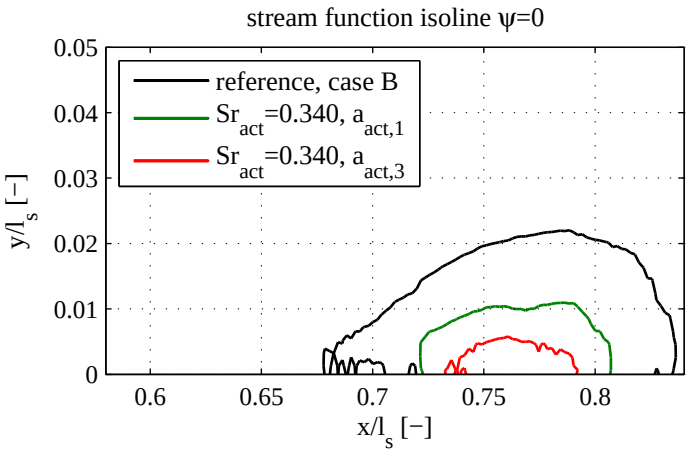

FIGURE 9. SEPARATION STREAMLINES FOR CASE B, $Sr_{\text{act}} = 0.340$ *(dissimilar scale)*

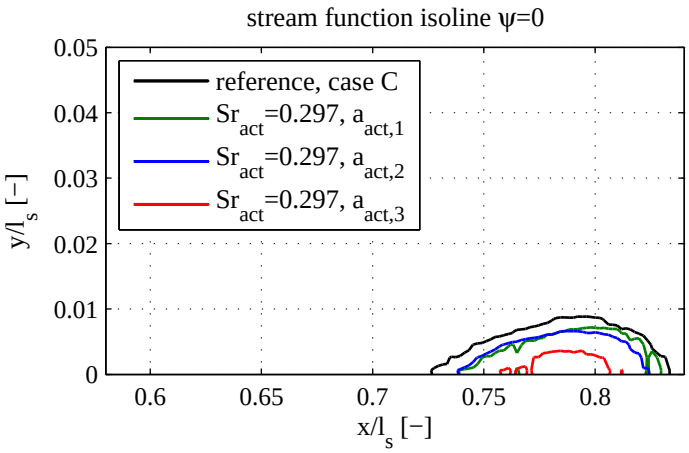

FIGURE 10. SEPARATION STREAMLINES FOR CASE C, $Sr_{\text{act}} = 0.297$ *(dissimilar scale)*

have been made for cases B and C. The resulting border streamlines for the optimal frequency in each case are plotted in Fig. 9 and 10. The presented results confirm the finding that the effect can be enlarged by an increase of actuation amplitude. In comparison to case A the separation point for both cases, B and C, is moved further downstream. This can be explained by the wind tunnel mode of operation. With a boundary layer suction in the acceleration of the contoured wall, the separation is forced onto the opposite flat plate. If the suction is too strong, the generated pressure field still forces the boundary layer to separate early. For cases B and C this suction was smaller and likewise the forcing pressure gradient. This allows the actuation to reduce the bubble size while moving the separation point further downstream.

The reduction of separation is largest for case B, where the height of the bubble is reduced to approximately 27 % and its

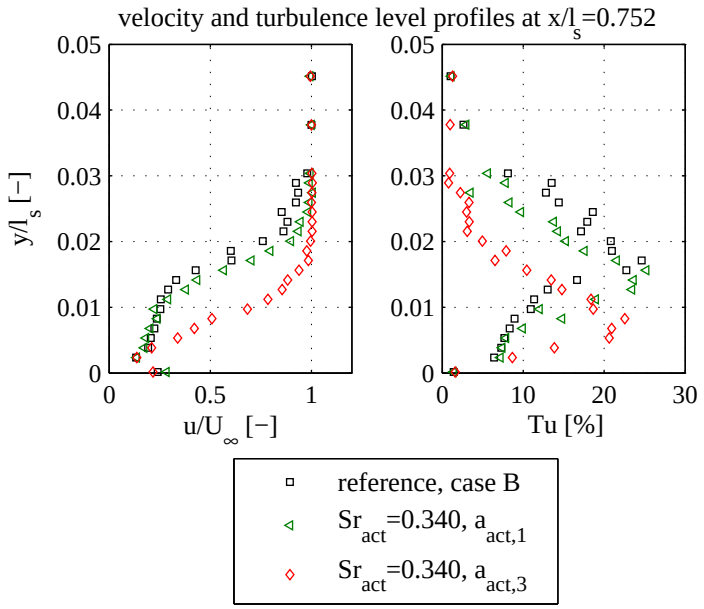

FIGURE 11. VELOCITY AND TURBULENCE LEVEL PROFILES FOR CASE B, $Sr_{\text{act}} = 0.340$

length is shortened to about 36 % (see Fig. 9). The strong adverse pressure gradient in case A impedes the actuation effectiveness. Therefore actuation is most effective in case B.

Velocity Profile and Turbulence Level

Information about the changing velocity profile and the corresponding turbulence level with actuation can be obtained by the use of hot wire measurements. The results of a 90° *Dantec-Dynamics* 55P14 hot wire probe traverse in the separated zone at $\tilde{x} = 0.752$ are shown in Fig. 11. The measurements were taken for case B in the reference flow field and for the actuation frequency $Sr_{\text{act}} = 0.340$, found to be most effective by means of PIV. In the diagram on the left hand side the dimensionless velocity is plotted. As expected from the PIV results, the boundary layer gets smaller with actuation. The turbulence level is displayed on the right hand side of Fig. 11. It is approximately 1 % in the free stream and its peak in the separation is $Tu \approx 25\,\%$. With actuation the shape of the turbulence level profile becomes more like that of an attached boundary layer where Tu would be monotonically decreasing from a certain distance from the wall to free stream. The height of the separation bubble, which is indicated by the maximum of the turbulence level, hence is decreased from 0.018 in the reference case (black squares) to 0.009 for $\tilde{a}_{\text{act},3}$ (red diamonds). The hot wire measurements thus confirm that the separation bubble can be reduced by means of actuation.

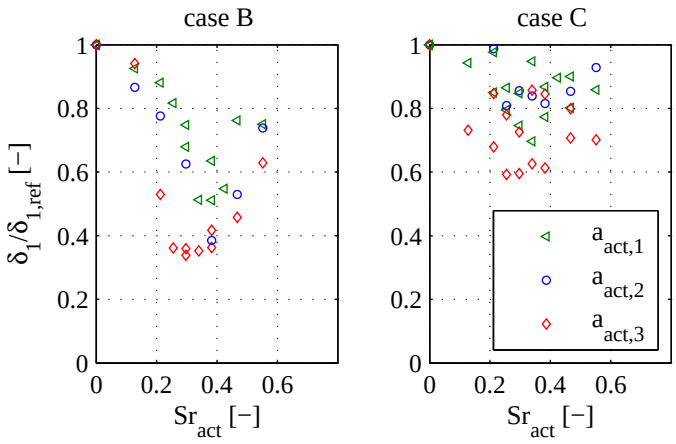

FIGURE 12. COMPARISON OF $\delta_1/\delta_{1,ref}$ FOR DIFFERENT ACTUATION CONFIGURATIONS

Summary of Present Results

A summary of the measurements for case B and C is shown in Fig. 12. The reduction of the maximum value of δ_1 related to the maximum of the reference case $\delta_{1,ref}$ is used as a measurement for actuation effectiveness. In the left hand diagram the values for case B are displayed. It can be found that the ratio $\delta_1/\delta_{1,ref}$ is diminishing with increasing actuation amplitude. The highest reduction to approximately 35 % thereby is achieved at a Strouhal number of $Sr_{\text{act}} \approx 0.297 - 0.340$.

For case C the relative reduction of displacement thickness is smaller than for case B. The reason for this is the very small reference bubble size. The most effective actuation for this case takes place at $Sr_{\text{act}} \approx 0.297$ where the displacement thickness is reduced to 60 %.

These findings confirm the numerical investigations of Rist and Augustin [12] and Ries et al. [15, 16] who describe the separation bubble control by means of actuation.

To compare the findings to those of other authors, energy has to be addressed. Energy is proportional to the square of velocity. Thus, the energy needed for actuation the way it is described in this paper is small compared to that for vortex generating jets. According to Bons et al. [9] blowing ratios of $u_{jet}/U_\infty = 0.5$ to 2.0 are common for VGJs, while in this study the blowing ratio is only $\tilde{a}_{act,1} = 0.05$ to $\tilde{a}_{act,3} = 0.3$ high. Squaring the maximum ratio of this study, the energy can be reduced to a third of the energy that is needed using the lowest blowing ratio for VGJs. Additionally, as the experimental setup demonstrates, no mass flow is needed at all. The pulse transported by the diaphragm underneath the slot is sufficient for actuation.

Ensemble-Averaged PIV Results

A phase-logged data acquisition permits the investigation of the boundary layer behaviour related to actuation frequency.

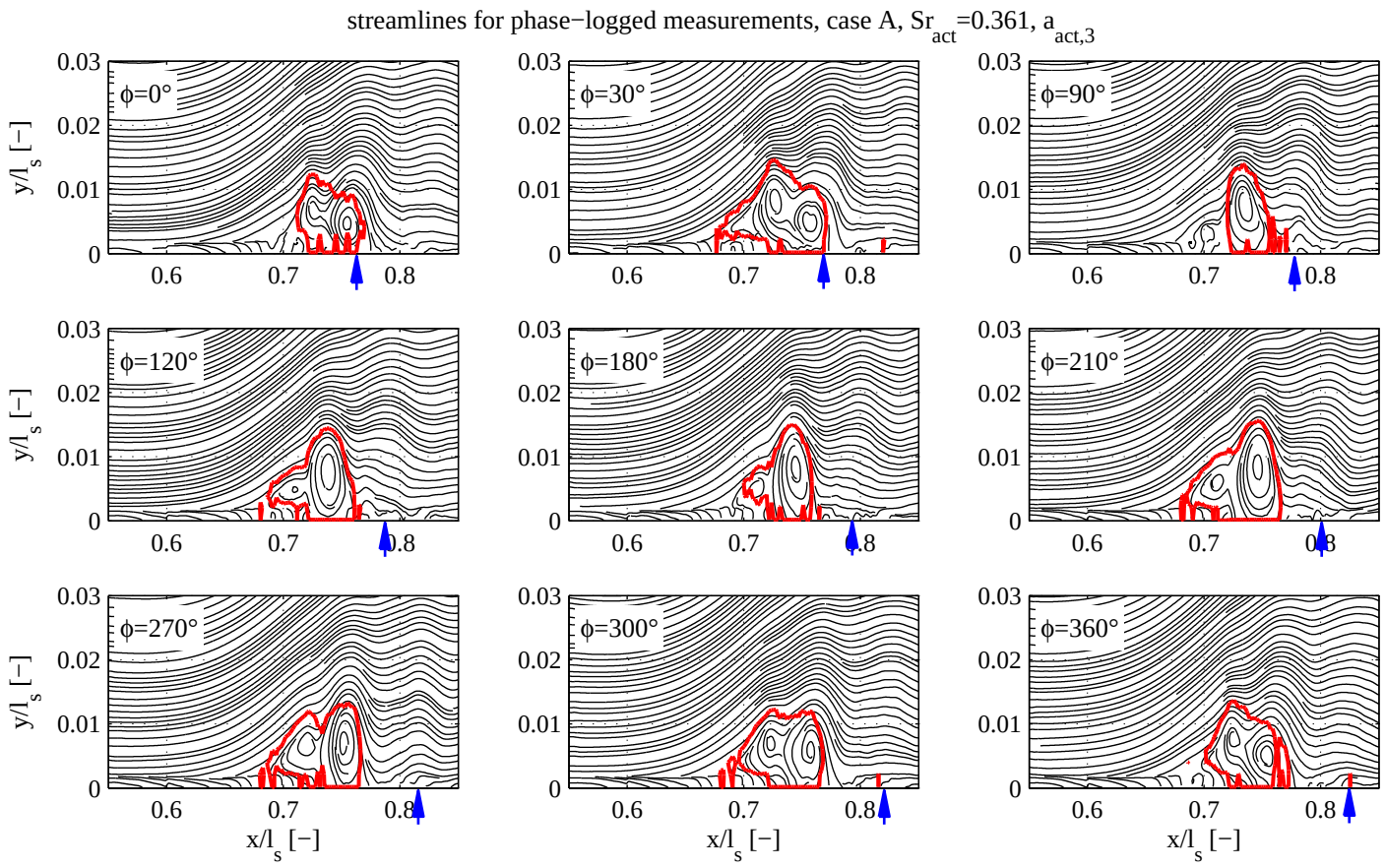

FIGURE 13. STREAMLINE PLOTS FOR DIFFERENT PHASE ANGLES FOR CASE A, $Sr_{\mathrm{act}} = 0.361$, $\tilde{a}_{\mathrm{act},3}$ *(dissimilar scale)* The streamlines were plotted using the *streamslice* function from *MATLAB*.

Flow structures that are driven by the inserted frequency can be detected. For that purpose ensemble-averaged PIV measurements have been taken. An example can be found in Fig. 13 where streamlines for different phase angles are presented. In all subpictures coherent structures can be seen from the point of separation to the end of the observation window. These structures have a vortical character in the separation bubble, pictured with the corresponding separation streamline (thick red line). These structures still can be seen downstream of the reattachment point where they have a wave form. This can be explained by the increase of fluid speed at reattachment. The reverse flow in the vortices after this speed-up is not high enough to actually be reverse flow. In this case there is only a wave moving along the flat plate instead of a vortex. Additionally, vorticities outside the separation are overlain with random scatter and thus are eliminated by the averaging process.

The vortex at $\tilde{x} = 0.76$ in the picture for a phase angle of $\phi = 0\,^\circ$ moves downstream with increasing phase angle. This is also true for the wave crest in the streamlines on top of it. The vortex disappears from $30\,^\circ$ to $90\,^\circ$ where according to the separation streamline it has left the separated zone. Yet, its influence on the streamlines still can be tracked in the following pictures (blue arrow). In the phase diagram of $\phi = 120\,^\circ$ a new vortex is forming at about $\tilde{x} = 0.7$. It is growing and moving downstream in the pictures to $\phi = 300\,^\circ$, where it has reached the size of the first vortex and finally to $360\,^\circ$, where the new vortex has overgrown the first one.

Starting this study, the amplification of Tollmien-Schlichting instabilities was targeted. With the findings from the phase-averaged PIV measurements the Kelvin-Helmholtz (K-H) instabilities are more likely to dominate the actuated flow behaviour. This can be assumed as the diagrams in Fig. 6 indicate no variation of the boundary layer parameters upstream of the separation due to actuation. The velocity profiles int the PIV pictures likewise do not alter significantly.

To confirm the presence of K-H instabilities, the flow will be investigated in further studies.

CONCLUSION

In this paper the effect of actuation on a laminar separation bubble was investigated. Actuation in this context means the introduction of a pressure pulsation into a flat plate boundary layer simulation of an LP turbine suction side. The pulsation at a certain frequency is introduced through a slot, sealed with a thin diaphragm, and promotes the Kelvin-Helmholtz instability of the shear layer of the separation. The bubble is suppressed and reduced aerodynamical loss is expected in the turbine context.
By means of PIV measurements three different reference bubble sizes have been investigated. The actuation Strouhal number Sr_{act} therefore was varied from $0.2-0.5$ for three actuation amplitudes. In most cases the actuation has a reducing effect on the bubble. This reduction is found to be dependent on Strouhal number and amplitude as follows.

1) Within a certain range the effect of Sr is only weak. Yet, Strouhal numbers that are too low or too high considerably lessen the actuation effectiveness. For $Re \approx 60,000$ the most effective Strouhal number range was $0.297 \leq Sr_{\text{act}} \leq 0.382$.
2) The actuation amplitude has a major effect on separation reduction. The largest effect for all cases is gained with the highest amplitude, which is equivalent to blowing ratio, of $a_{\text{act},3}/U_\infty = \tilde{a}_{\text{act},3} \approx 0.3$.
3) The maximum reduction is achieved with a Strouhal number of $Sr_{\text{act}} = 0.340$ and an amplitude of $\tilde{a}_{\text{act},3} = 0.3$. The separation is reduced to approximately 27 % in height and about 36 % in length which leads to a reduction to a tenth of the reference separation bubble size.

The conclusion is that the boundary layer actuation is successful. A major reduction of separation bubble size is achieved by only a third of the energy, relative to free stream kinetic energy, needed for pulsed vortex generating jets. Further investigations are planned to gain more insight in the physical processes that underly the presented effects.

ACKNOWLEDGMENT

The financial support from the *VITAL* funding in the very early phase of this project is acknowledged.

REFERENCES

[1] Ardey, S., Gier, J., and Huebner, N., 2000. "Kostenreduktion durch neue Aerodynamische Konzepte bei Niederdruckturbinen". In *Deutscher Luft- und Raumfahrtkongress, Jahrbuch 2000*, Vol. 1. DGLR.

[2] Himmel, C. G., Thomas, R. L., and Hodson, H. P., 2009. "Effective Passive Control for Ultra-High-Lift Low Pressure Turbines". In European Turbomachinery Conference, March 23-27, 2009, Graz, Austria.

[3] McAuliffe, B. R., and Yaras, M. I., 2009. "Passive Manipulation of Separation-Bubble Transition Using Surface Modifications". *Journal of Fluids Engineering,* ***131***, pp. 021201–1–021201–16.

[4] Schumann, T., Rose, M. G., Staudacher, S., Gier, J., and Schroeder, T., 2008. "The Effects of Steady Injection on an Ultra High Lift Vane in a LP Turbine". In ASME Turbo Expo, Power for Land, Sea and Air, June 9-13, 2008, Berlin, Germany. GT2008-50330.

[5] Volino, R. J., 2003. "Separation Control on Low-Pressure Turbine Airfoils Using Synthetic Vortex Generator Jets". In ASME Turbo Expo, Power for Land, Sea and Air, June 16-19, 2003, Atlanta, Georgia, USA. GT2003-38729.

[6] Rivir, R. B., Sondergaard, R., Bons, J. P., and Yurchenko, N., 2004. "Control of Separation in Turbine Boundary Layers". In 2nd AIAA Flow Control Conference, June 28 - July 1, 2004, Portland, Oregon, USA. AIAA 2004-2201.

[7] Gross, A., and Fasel, H. F., 2004. "Active Control of Separation for Low-Pressure Turbine Blades". In 2nd AIAA Flow Control Conference, June 28 - July 1, 2004, Portland, Oregon, USA. AIAA 2004-2203.

[8] Bons, J. P., Hansen, L. C., Clark, J. P., Koch, J., and Sondergaard, R., 2005. "Designing Low-Pressure Turbine Blades with Integrated Flow Control". In ASME Turbo Expo, Power for Land, Sea and Air, June 6-9, 2005, Reno, Nevada, USA.

[9] Bons, J., Reimann, D., and Bloxham, M., 2008. "Separated Flow Transition on an LP Turbine Blade with Pulsed Flow Control". *Journal of Turbomachinery,* ***130***, pp. 021014–1–021014–8.

[10] Volino, R. J., Kartuzova, O., and Ibrahim, M. B., 2009. "Experimental and Computational Investigations of Low-Pressure Turbine Separation Control Using Vortex Generator Jets". In ASME Turbo Expo, Power for Land, Sea and Air, June 8-12, 2009, Orlando, Florida, USA. GT2009-59983.

[11] Stieger, R. D., and Hodson, H. P., 2003. "Unsteady Dissipation Measurements on a Flat Plate Subject to Wake Passing". *Transactions of the ASME,* ***127***, April, pp. 388–394.

[12] Rist, U., and Augustin, K., 2005. "Control of Laminar Separation Bubbles Using Instability Waves". In ISABE, 17th Symposium on Air Breathing Engines, September 4-9, 2005, Munich, Germany. ISABE-2005-1041.

[13] Ricci, R., Montelpare, S., and Silvi, E., 2007. "Study of Acoustic Disturbances Effect on Laminar Separation Bubble by IR Thermography". *Experimental Thermal and Fluid Science,* ***31***, pp. 349–359.

[14] Lang, M., 2005. "Experimentelle Untersuchungen zur Transition in einer laminaren Abloeseblase mit Hilfe der Laser-Doppler-Anemometrie und der Particle Image Velocimetry". PhD thesis, Universitaet Stuttgart.

[15] Ries, T., Baumann, J., Rose, M. G., Staudacher, S., and

Raab, I., 2009. “LP Turbine Laminar Separation Bubble Study: Flat Plate DNS Calculations and Preliminary PIV Data”. In European Turbomachinery Conference, March 23-27, 2009, Graz, Austria.

[16] Ries, T., Mohr, F., Baumann, J., Rose, M. G., Rist, U., Raab, I., and Staudacher, S., 2009. “LP Turbine Laminar Separation with Actuated Transition; DNS, Experiment and Fluidic Oscillator CFD”. In ASME Turbo Expo, Power for Land, Sea and Air, June 8-12, 2009, Orlando, Florida, USA. GT2009-59600.

[17] Baumann, J., Ries, T., Rose, M. G., Rist, U., and Staudacher, S., 2009. “Actuated Transition in LP Turbine Laminar Separation - an Experimental Approach”. In Deutscher Luft- und Raumfahrt Kongress, September 8-10, 2009, Aachen, Germany. DLRK2009-121277.

[18] Schlichting, H., 1965. *Grenzschicht-Theorie*. Verlag G. Braun, Karlsruhe.